Optoelectrochemical Transduction on Planar Optical Waveguides

C.Piraud, E.K.Mwarania, J.Yao#, K.O'Dwyer*, D.J.Schiffrin*, & J.S.Wilkinson

Optoelectronics Research Centre

The University

Southampton

SO9 5NH

UK

Tel: 44 703 592792

*Department of Chemistry

The University of Liverpool

PO Box 147

Liverpool

L69 3BX

UK

Tel: 44 51 794 3574

#Now with the Department of Electronic & Electrical Engineering, King's College London, The Strand, London, WC2R 2LS, UK. Tel: +44 71 836 5454 ext. 1227.

Abstract.

Planar optical waveguides overlaid with electrochemically-modulated sensing films comprise a powerful new class of chemical transducer. In this paper, the effects upon the modal absorption spectrum of depositing a highly absorbing electrochromic film on an optical waveguide are modelled. Theoretical and experimental results are given for such a device consisting of a lutetium biphthalocyanine film deposited on an indium tin oxide-coated potassium ion-exchanged glass waveguide, for application as a chlorine sensor.

1. Introduction.

Planar optical waveguides show much promise in the realisation of novel chemical and biological sensors which use the interaction of evanescent fields with specifically sensitised films on the waveguide surface. Such sensors may probe changes in the refractive index of films using surface plasmon resonance [1], light emission from the binding of proteins labelled with fluorophores [2], or the change in absorption spectrum of a film caused by a chemical reaction [3], for example. The technology of integrated optics allows photolithographic replication of complex mass-produced multisensors on small, robust, substrates, and electrochemical techniques allow electrical resetting of reactions, or improved sensitivity through Stark modulation and phase-sensitive detection.

In this paper theoretical and experimental results relating to an electrochemically modulated evanescent absorption sensor are described. It has been found that the loss spectrum of a guided mode in a waveguide coated with a highly absorbing film is substantially shifted in wavelength when compared with the bulk absorption spectrum. A computer simulation is used to model these waveguides, and show how bulk and waveguide absorption spectra are related. In particular it is shown how the waveguide absorption spectrum changes with the magnitude of the bulk absorption, with buffer layer thickness, and with sensing film thickness. It is shown that a buffer layer between waveguide and sensing film is required to reduce the interaction strength and obtain losses low enough to yield measurable output signals.

In the computer model the real part of the index of the sensing film is deduced from a measured or simulated absorption spectrum using the Kramers-Kronig relations. The films being studied have strong absorption peaks and, consequently, the real part of index dips substantially on the short-wavelength side of the absorption peak and rises to a peak on the long-wavelength side. The electromagnetic boundary conditions at the interface between the sensing film and the analyte are substantially different for the TE and TM modes and thus it is found, for thin sensing films, that the TE and TM modes propagating in the waveguides exhibit very different behaviour. The TM mode is dominated by enhanced absorption due to the increase in optical field strength at the sensing film/electrolyte interface at the wavelength where the index dips, while the TE mode is dominated by enhanced absorption at the wavelength where the index is maximum.

The absorption spectrum of lutetium biphthalocyanine films in both the green (reduced) and red (oxidised) states have been measured using a dual-beam spectrophotometer, and the above computer model used to design a suitable waveguide structure to probe such films. This device has been constructed, and waveguide loss spectra are given and compared with theoretical predictions. In a further paper, the use of this device as a electrically regenerable chlorine sensor is described [4].

2. Theoretical modelling.

2.1 Computer simulation of the multilayer structure.

The imaginary part of the propagation coefficient (or of the effective index) of a guided mode may be used to determine waveguide loss, in the same way as the absorption of a bulk material is related to the imaginary part of the index of that material. To find the waveguide loss of a waveguide coated with a thin film of such material from the bulk absorption, the waveguide eigenvalue equation must be solved, by satisfying wave equations in each of the media comprising the device and by matching tangential components of electric and magnetic fields at the boundaries. Guided-mode solutions are found when the fields decay to zero outside the guiding structure. Numerical techniques have been used to obtain the results given in this paper, as the structures being analysed are multilayer, consisting of a waveguide film, a buffer layer, a transparent conducting film, and a sensing film (Table 1). A matrix method described by Yeh [5] has been employed, in which 2x2 matrices are derived from the boundary conditions for the fields at each dielectric interface, and are multiplied together. A guided mode solution is found when one coefficient of the resultant matrix becomes zero, representing a guided mode where evanescent fields decay to zero an infinite distance away from the guide, normal to the dielectric interfaces. This coefficient is a function of wavelength, and the film thickness and complex index of each layer. Mullers method [6] is used to find this condition, as the equation involved is complex.

The computer model determines the waveguide loss as a function of wavelength in dB/cm, for TE or TM modes of the slab structure. All layers are assumed to extend

infinitely in the plane of the substrate: no attempt has been made to model channel waveguides. In this model, the index only varies with wavelength in the sensing film. It is expected that the effect of material dispersion in the other layers, which has thereby been neglected, will be negligible compared with the strong variation of index with wavelength of the sensing film.

2.2 Modelling of the complex index of the sensing film.

Before applying this model to experimental data for the bulk absorption of a real material, as described in section 4, a theoretical Gaussian absorption spectrum was used to simulate a peak in the imaginary part of index, in order to study the general properties of these devices.

The complex refractive index of the sensing film is defined as
$n = n' - jK$. In this section a single absorption peak is modelled by:

$$K(\lambda) = A \; exp\left[-\left(\frac{\lambda - \lambda_p}{\delta} \right)^2 \right] \qquad (1)$$

where A is the absorption magnitude

λ is the wavelength

λ_p is the peak absorption wavelength

2δ is the absorption bandwidth, measured at 1/e points

and the real part of index is calculated using Kramers-Kronig relations [7]:

$$n'(\omega_0) = 1 + \frac{2}{\pi} P \int_0^{\infty} \frac{\omega K(\omega)}{(\omega^2 - \omega_0^2)} d\omega \qquad (2)$$

where ω is the angular frequency, and where P indicates that the Cauchy principal integral is taken at $\omega = \omega_0$, and $K(\omega)$ must be analytic in the upper half of the complex plane.

The real part of index derived from a single absorption peak, using Eqn. 2, has omitted from it the effects of other absorption peaks, particularly in the UV. In particular, a large offset in the real part of index will be neglected. To obtain a realistic model an additional absorption peak at 250nm, of magnitude $A_{uv} = 50$ and bandwidth $2\delta = 100$nm, has been added to the absorption spectrum in all our calculations to shift n' to a typical value of between 1.5 and 1.9 at the wavelength of peak absorption. The centre wavelength of this UV absorption was chosen arbitrarily to model the physical phenomena resulting in elevated index. Choice of a different wavelength would have modified the slope of the n' curves slightly.

Figure 1 shows the real part of index, calculated using Eqn.2, for different absorption magnitudes, A = 0.1, 0.5, & 1.0; the imaginary part, K, is only shown for A = 1.0. The centre wavelength, λ_p, in each case is 660nm and the absorption bandwidth, 2δ, is 60nm. These values are comparable with the absorption spectra of the biphthalocyanines [8]. Figure 1 shows that when the absorption is large, for example when A = 1, n' dips substantially at a wavelength shorter than the wavelength of maximum absorption, but

within the absorption band.

2.3 Waveguide parameters

The parameters describing the other layers in the waveguide device were given the values in Table 1. These values approximately model potassium ion-exchanged waveguides in soda-lime glass, coated with a silica buffer layer and a thin indium tin oxide (ITO) electrode. The device is assumed to be immersed in water.

Layer	Index	Thickness
Substrate	1.51 +j0	
Guide	1.52 +j0	3 μm
Silica buffer	1.458 +j0	200 nm
ITO electrode	2.00 +j0	10 nm
Sensing film	see fig 1	10 nm
Superstrate	1.33	

Table 1. Waveguide parameters.

3. Theoretical results.

3.1 Magnitude of sensing film absorption.

Figure 2 shows the waveguide loss of the above structure plotted as a function of wavelength for three values of absorption magnitude, A, corresponding to the three bulk index curves shown in Figure 1. Figures 2a & 2b give the loss for the TE_0 and TM_0 modes of the structure, respectively.

Consider first the TE mode. For small absorption strengths, the wavelength of peak absorption coincides with that of the bulk material. However, this wavelength increases as peak absorption strength increases, because the modal field distribution changes as a function of sensing film index and therefore of wavelength. This effect increases the overlap of guided power with the sensing film when n' is large, at wavelengths longer than the absorption peak. The reduction in absorbtance with wavelength is thereby balanced by an increase in the power in the film available to be absorbed, resulting in a shift in the wavelength at which the combination is maximised.

For small bulk absorption, A = 0.1, the modal absorption behaviour of the TM mode, shown in Figure 2b, is similar to that of the TE mode. However, as the peak absorbtance increases, the modal absorption spectrum changes, the peak shifting to shorter, rather than longer, wavelengths. This occurs because, as A increases, the index of the sensing film dips further at a wavelength shorter than the bulk material absorption peak, as shown in Figure 1. At this wavelength the field strength at the interface between the sensing film and the water superstrate increases for the TM polarisation with increasing

A.

3.2 Effect of UV absorption.

Figures 3a & 3b show the effect on modal absorption spectrum of varying the uv absorption at 250nm (A_{uv} = 10, 20, & 50; δ = 50nm), for the TE_0 & TM_0 modes respectively. A (at 660nm) is taken to be 1.0, and all other parameters are as in Table 1. The principal effect of this upon the complex index, in the wavelength range of interest, is an overall increase in n' with increasing A_{uv}. Figure 3a shows that the peak absorption of the TE mode rises with increasing n', as the modal field profile changes, increasing the power travelling in the sensing film. The behaviour of the TM mode, shown in Figure 3b, is reversed; as n' increases, the dominance of the surface field enhancement due to the dip in n' reduces, reducing the power travelling in the sensing film, lowering the peak modal absorption and tending to shift the absorption peak back towards 660nm.

Taken to an extreme, for materials such as silver where the real part of index is close to zero at visible wavelengths, the TM mode may have an extremely high absorption due to the existence of a surface plasma wave [1] at the silver surface.

3.3 Thickness of the silica buffer.

Figure 4 shows the effect upon the peak modal absorption of varying the thickness of the silica buffer for the TE and TM modes. A is taken to be 1.0, and all other parameters are as in Table 1. The thickness of silica has no effect upon the location of the modal

absorption peak for the thicknesses shown here. As expected, the absorption strength decreases with thickness of silica buffer, as the evanescent field decays further before it encounters the sensing film. Using these curves, the silica thickness required to give the waveguide absorption required for a particular device design may be determined. The inclusion of a silica buffer between the waveguide and the ITO film will also have the effect of reducing any spurious losses due to ITO film absorption.

3.4 Thickness of the sensing film.

Figures 5a & 5b show the effect upon the modal absorption spectrum of varying the thickness of the sensing film for the TE and TM modes, respectively. A is taken to be 1.0, and all other parameters are as in Table 1. In the case of the TE mode, increasing thickness has a similar effect to increasing A; the peak modal absorption increases, as more power travels in the film, and the wavelength at which this peak occurs increases. The TM modal absorption spectrum is affected in a similar way, but again the wavelength at which TM peak modal absorption occurs decreases with film thickness.

3.5 Discussion of the theoretical model.

It is clear from the discussion above that the modal spectral absorption of waveguides coated with highly absorbing films is not straightforwardly related to the bulk absorption spectrum, due to the strong variation of the mode field profile with complex index and therefore with wavelength. In many applications, information about sensing films obtained by using both TE and TM polarisations will be useful. However, it has been seen that, depending upon the real part of the film index, the two polarisations may exhibit

substantially different losses. The TM mode being dominated by the minimum in n', and the TE mode being dominated by the maximum. It is therefore necessary to perform careful modelling of this type of waveguide device to obtain a structure in which both polarisations may readily be probed. It has also been shown that a silica buffer layer may be used to o' tain the desired range of waveguide output powers for simple detection.

4. Design & realisation of a waveguide probe for lutetium biphthalocyanine.

The above computer model was used to design a multilayer waveguide device coated with a thin film of lutetium biphthalocyanine {$Lu(PC)_2$}. $Lu(PC)_2$ is an electrochromic material whose absorption spectrum changes depending on redox state. On oxidation it changes from the green to the red form and this reverses on reduction. These reactions may be performed by applying suitable potentials between an electrolyte and an electrode, such as ITO, upon which a thin film of $Lu(PC)_2$ has been deposited. Oxidation may also occur through reaction with chlorine in solution, which is the basis of a resettable chlorine sensor [4].

4.1 The complex index of $Lu(PC)_2$.

Electrochemical experiments were carried out in situ, in spectrophotometer cells. The working electrode was an ITO film onto which a $Lu(PC)_2$ film had been deposited by vacuum evaporation. The counter electrode was a platinum wire placed in the solution, and a silver wire covered with silver chloride was used as the reference electrode. These last two electrodes were placed in the spectrophotometer cell outside the light path. The

Ag/AgCl electrode was prepared by anodising the silver wire in a KCl solution prior to the experiment.

Figure 6 shows the cyclic voltammetry of the film electrode in 0.05M NaCl. As previously observed [8], the first voltammogram differs significantly from the steady-state response. The oxidation wave observed at approximately 0.65V corresponds to the green-red transition and the corresponding reduction is observed at approximately 0.5V. The difference in oxidation and reduction potentials indicates some degree of irreversibility in the redox chemistry in neutral solutions [8], but this has no effect upon the optical constants of the film, provided that the applied potential is sufficiently removed from the region of the transition.

The bulk absorbtance of a $Lu(PC)_2$ film electrode was measured in a Pye Unicam SP8-100 spectrophotometer. A 40nm thick film of $Lu(PC)_2$ was deposited by vacuum evaporation on a glass microscope slide coated with ITO, and immersed in a 0.05M NaCl solution. The reference cell of the spectrophotometer contained a similar ITO-coated slide placed in the same solution. Figure 8a shows the absorption spectrum of the $Lu(PC)_2$ in the reduced state at 0V and Figure 8b shows the spectrum of the same sample in the oxidised state at 0.7V. The spectra are taken over a broad wavelength range to improve the accuracy of subsequent calculations using the Kramers-Kronig relations. As can be seen, significant differences in the absorption spectrum are observed: the peaks at 660nm and 1300nm are reduced, and the peak at 920nm is enhanced. The magnitude of the absorbtance was independent of time, showing that complete reduction and oxidation was achieved at the potentials employed.

The imaginary part, K, of the complex index of this film was then calculated from the absorbtance, the peak value in the green state being K = 0.76 at a wavelength of 660nm, and the real part was deduced from this using the Kramers-Kronig relations as before; the resultant complex index is shown in Figures 9a & b, for the green and red form, respectively. Before deducing n' from K, UV absorption was modelled by adding a Gaussian absorption peak (A_{uv} = 50; δ = 50nm) at a wavelength of 250nm. The amplitude of this peak was that required to shift n' to a typical value (n' = 1.6) for the phthalocyanines [9] at the wavelength of peak absorption in the green form. No data is available for the refractive index of $Lu(PC)_2$, but it is expected that the presence of a lutetium centre will not significantly affect the values of index given in reference 9.

4.2 Modelling of $Lu(Pc)_2$-coated waveguides.

A $Lu(Pc)_2$-coated waveguide was then modelled using the above spectroscopic data and the values for waveguide parameters given in Table 1. The predicted modal absorption spectra for the reduced and oxidised forms are shown in Figures 9a & b, respectively, for both the TE and the TM polarisations. It can be seen that the wavelengths of peak absorption are slightly shifted with respect to the bulk absorbtance and that the TE modal absorption is higher than that of the TM mode, as expected. In addition, it appears that for the TE mode, the absorption peaks at longer wavelengths are enhanced.

4.3 Fabrication of $Lu(Pc)_2$-coated waveguides.

Single-mode waveguides were fabricated in a soda-lime glass slide by ion-exchange in

molten KNO_3 at 392°C for 1 hour [10]. A 200nm thick silica film was deposited on the waveguides by RF sputtering in an argon atmosphere. A 10nm thick ITO film was then deposited by reactive evaporation in oxygen and was annealed in an atmosphere of cracked ammonia [11]. The sheet resistance of this film was 730 ohms/square. The 10nm thick Lu(PC)$_2$ film was then evaporated from a powder under high vacuum through a mask, to coat a 4.5mm length of the waveguides. A silica cell was attached to the substrate surface with silicone rubber, and filled with a 0.05M solution of NaCl. A silver/silver chloride reference electrode and a platinum counter electrode were placed in the cell for electrochemical control, and the films were cycled through oxidation and reduction four times prior to each optical measurement. The device configuration is shown in Figure 10.

4.4 Modal absorption spectrum measurements.

The waveguide loss of a typical waveguide was measured as a function of wavelength using the apparatus shown in Figure 11. Light from a white light source, passed through a monochromator, was launched into a single mode fibre, which was butted up to the channel waveguide under investigation. The light emerging from the waveguide was focused onto an avalanche photodiode (APD) through a polariser which was used to select either TE or TM polarisation. Spectral loss measurements were obtained by dividing the signal obtained in this way by that obtained directly from the input fibre, with the device removed. The typical loss obtained from fibre coupling to such a device was then subtracted from this insertion loss data, and the data then scaled to dB/cm for comparison with theoretical results. The final spectra are shown in Figure 12.

The measured modal absorption spectra for the TE polarisation agree well with the theoretical predictions in Figure 9. The magnitude and position of the absorption peaks are similar, with the exception that in the red form, the peak at 950nm appears to be substantially reduced in the experimental data.

The measured modal absorption spectra for the TM polarisation do not agree as well with theory, although the magnitude of the peak at approximately 670nm is approximately correct. The principal differences are that, in the experimental data, the absorption at long wavelengths is much greater than expected, and that there is an additional peak at 765nm; this peak is not substantially affected by the reduction and oxidation of the $Lu(PC)_2$ film, and its origin is unknown. The theoretical modelling performed in section 3.2 indicates that the enhancement of absorption for the TM polarisation, relative to the TE polarisation, may be due to a lower real part of index in the $Lu(PC)_2$ film than used in our model, at longer wavelengths.

Both the theoretical and the experimental results show that this device may be used as a sensitive electrochemically resettable sensor to monitor oxidation of $Lu(PC)_2$ by chlorine. The optimum wavelengths of operation are at approximately 680nm for the TE mode and 950nm for the TM mode. Careful modelling must be performed to find the optimum device design and operating wavelengths for each new sensing film material.

5. Conclusions.

Planar optical waveguides overlaid with electrochemically-modulated sensing films are potentially the foundation of a new range of powerful chemical multisensor for use in environmental and medical monitoring. We have theoretically investigated the interaction of highly absorbing thin sensing films with light propagating in a waveguide, to allow the design of sensors from spectroscopic data on the sensing film material. Differences between TE_0 and TM_0 mode behaviour, and between waveguide and bulk absorption spectra have been elucidated.

An example device, consisting of a thin film of $Lu(PC)_2$ on an indium tin oxide coated waveguide has been fabricated, and the electrochemically-controlled waveguide absorption spectra measured. These have been compared with theoretical predictions and reasonable agreement found. However, it is clear that the thickness of the sensing film must be very accurately controlled, and the bulk complex refractive index fully known, to obtain predictable behaviour. A description of a resettable optoelectrochemical chlorine sensor based upon this work is published elsewhere [4].

We have demonstrated that optoelectrochemical waveguide probes may be confidently designed for application with sensing materials, with known chemical and spectroscopic characteristics, which may be deposited on waveguides in thin film form.

Acknowledgements.

The authors would like to thank Dr.M.Jones and Dr.M.Wiles for assistance with electrochemical measurements, Dr.M.Hempstead for assistance with waveguide attenuation measurements, and Dr. G.Wylangowski for assistance in preparing the ITO films. This work was supported by the UK Science & Engineering Research Council.

References.

[1] H.J.M.Kreuwel, P.V.Lambeck, J.M.M.Beltman & Th.J.A.Popma, "Mode Coupling in Multilayered Structures Applied to a Chemical Sensor and a Wavelength-Selective Directional Coupler", Proc. 4th European Conference on Integrated Optics, May 11 - 13, 1987, pp. 217-220.

[2] A.N.Sloper, J.K.Deacon & M.T.Flanagan, "A Planar Indium Phosphate Monomode Waveguide Evanescent Field Immunosensor", Sensors & Actuators, B1, pp. 589-591, 1990.

[3] K.Nishizawa, E.Sudo, M.Maeda & T.Yamasaki, "Waveguide-Type Hydrogen Sensor", Proc. European Conf. Optical Communications, Barcelona, 1987, pp.99-102

[4] C.Piraud, E.K.Mwarania, G.Wylangowski, K.O'Dwyer, D.J.Schiffrin & J.S.Wilkinson, "An Optoelectrochemical Thin Film Chlorine Sensor Employing Evanescent Fields on Planar Optical Waveguides", submitted to Analytical Chemistry.

[5] P.Yeh, Optical Waves in Layered Media, Wiley, 1988.

[6] S.D.Conte & C.de Boor, Elementary Numerical Analysis, 3rd Edition, McGraw Hill, 1981.

[7] M.K.Debe, "Optical Probes of Organic Thin Films: Photons-In, Photons-Out", Progress in Surface Science, vol.24, nos.1-4, 1987.

[8] G.C.S.Collins & D.J.Schiffrin, "The Electrochromic Properties of Lutetium and other Phthalocyanines", J.Electroanal.Chem., 139, pp. 335-369, 1982.

[9] J.Martensson & H.Arwin, "Optical Characterisation of Thin Films of some Phthalocyanines by Spectroscopic Ellipsometry", Thin Solid Films, vol.188, pp.181-192, 1990.

[10] R.V.Ramaswamy & R.Srivastava, "Ion-Exchanged Glass Waveguides: A Review", Journal of Lightwave Technology, vol.6, pp.984-1002, 1988.

[11] L.Gupta, A.Mansingh & P.K.Srivastava, "Band-Gap Narrowing and the Band Structure of Tin-Doped Indium Oxide Films", Thin Solid Films, vol.176, no.1, pp.33-34, 1989.

Figure Captions.

Figure 1. Model of complex refractive index.

Figure 2. Theoretical waveguide absorption spectra for different sensing film absorbtances at 660nm. a) TE_0 mode; b) TM_0 mode.

Figure 3. Theoretical waveguide absorption spectra for different sensing film UV absorbtances. a) TE_0 mode; b) TM_0 mode.

Figure 4. Theoretical peak waveguide absorption vs silica thickness.

Figure 5. Theoretical waveguide absorption spectra for different sensing film thicknesses. a) TE_0 mode; b) TM_0 mode.

Figure 6. Cyclic voltammogram of $Lu(PC)_2$ film in 0.05M NaCl.

Figure 7. Absorption spectra of $Lu(PC)_2$ in green and red forms.

Figure 8. Calculated complex refractive index of $Lu(PC)_2$.
a) Green form; b) Red form.

Figure 9. Theoretical waveguide absorption spectra for $Lu(PC)_2$ -loaded waveguides.
a) TE_0 mode; b) TM_0 mode.

Figure 10. $Lu(PC)_2$ - loaded waveguide device with electrochemical cell.

Figure 11. Apparatus to measure waveguide absorption spectrum.

Figure 12. Experimental waveguide absorption spectra for $Lu(PC)_2$ - loaded waveguides. a) TE_0 mode; b) TM_0 mode.

Table Caption.

Table 1. Waveguide Parameters.

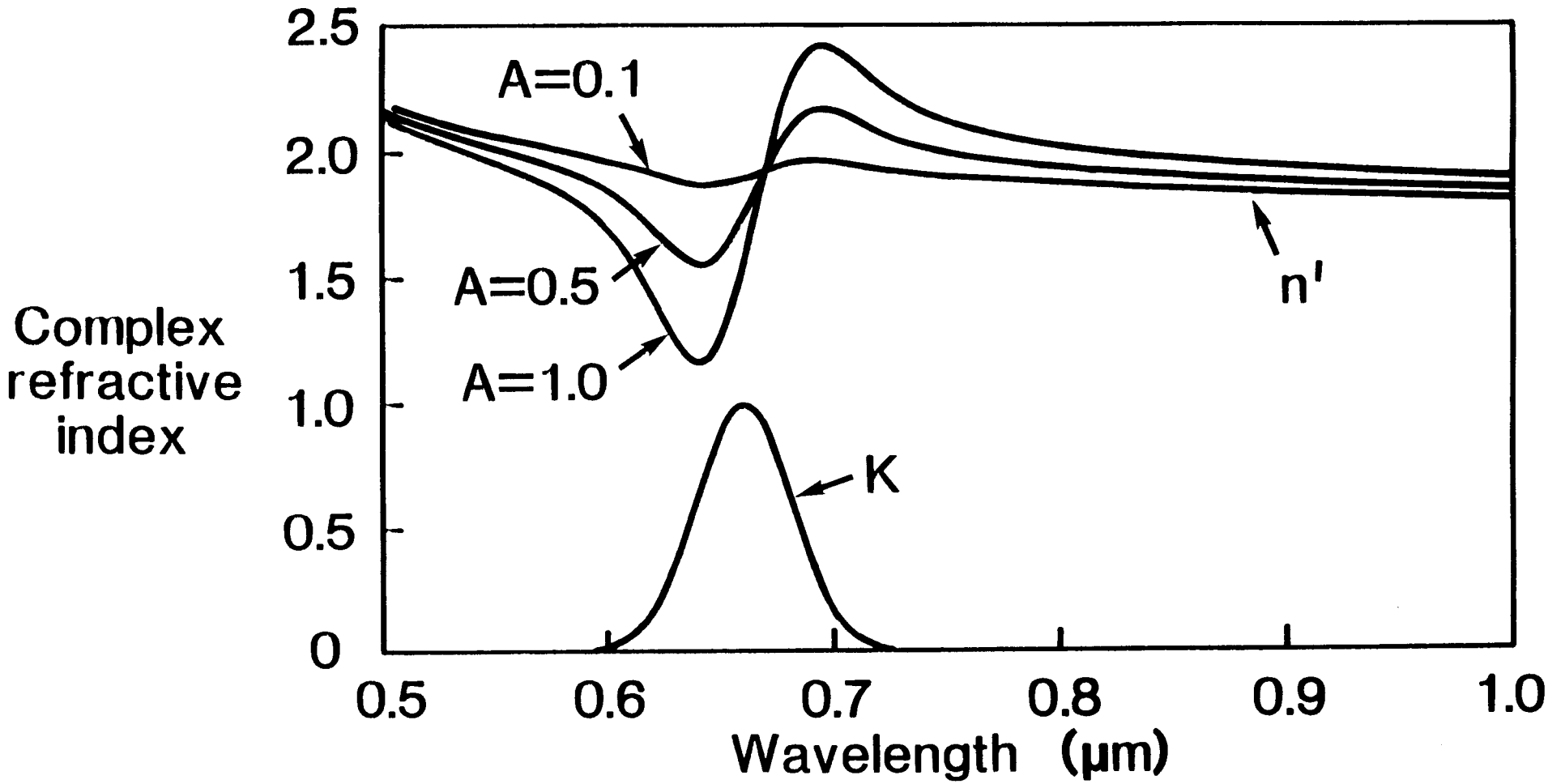
Complex refractive index
2.5
2.0
1.5
1.0
0.5
0
A=0.1
A=0.5
A=1.0
n'
K
0.5
0.6
0.7
0.8
0.9
1.0
Wavelength (μm)

Fig 1.

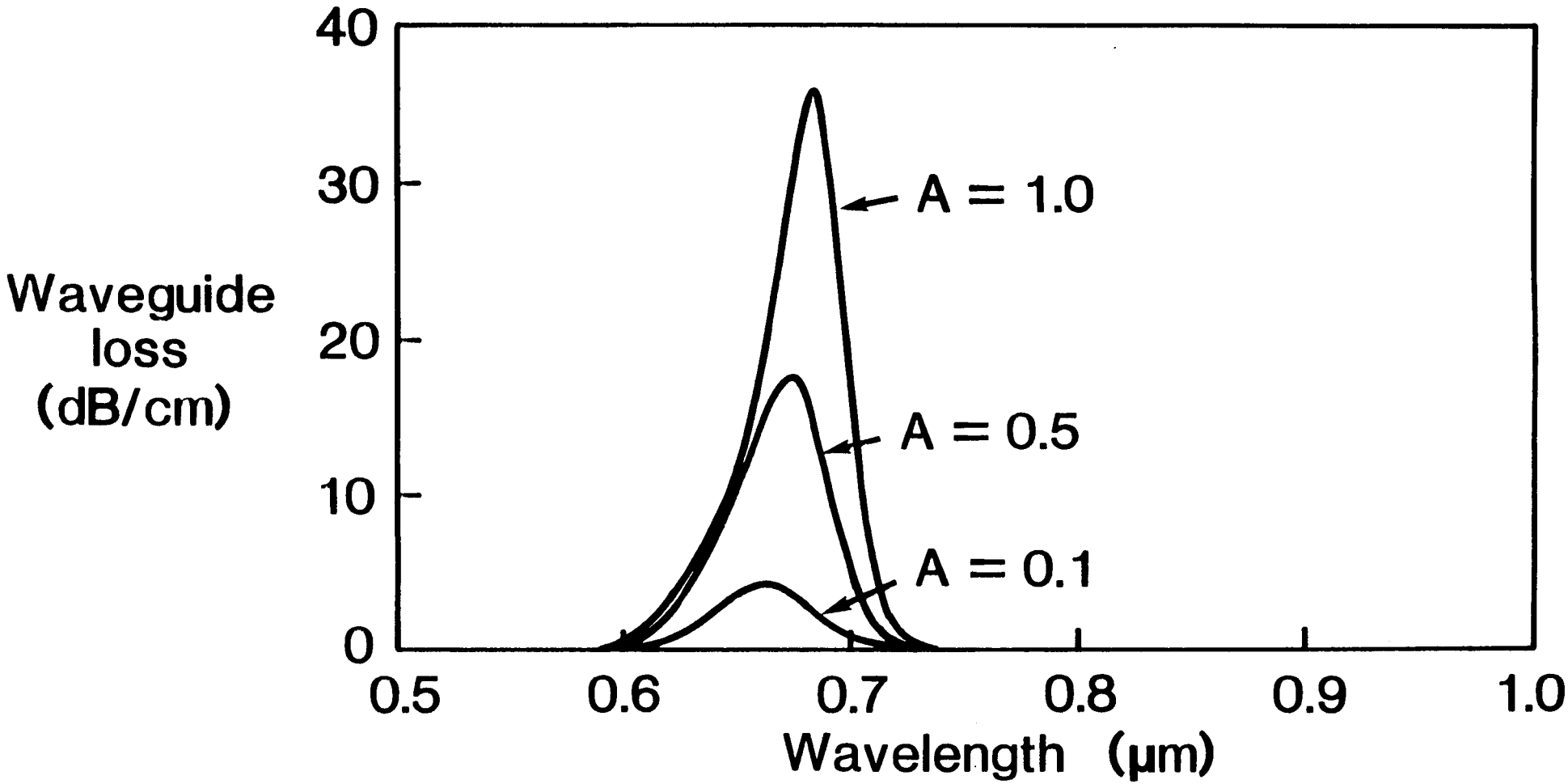
Waveguide loss (dB/cm)
40
30
20
10
0
A = 1.0
A = 0.5
A = 0.1
0.5
0.6
0.7
0.8
0.9
1.0
Wavelength (μm)

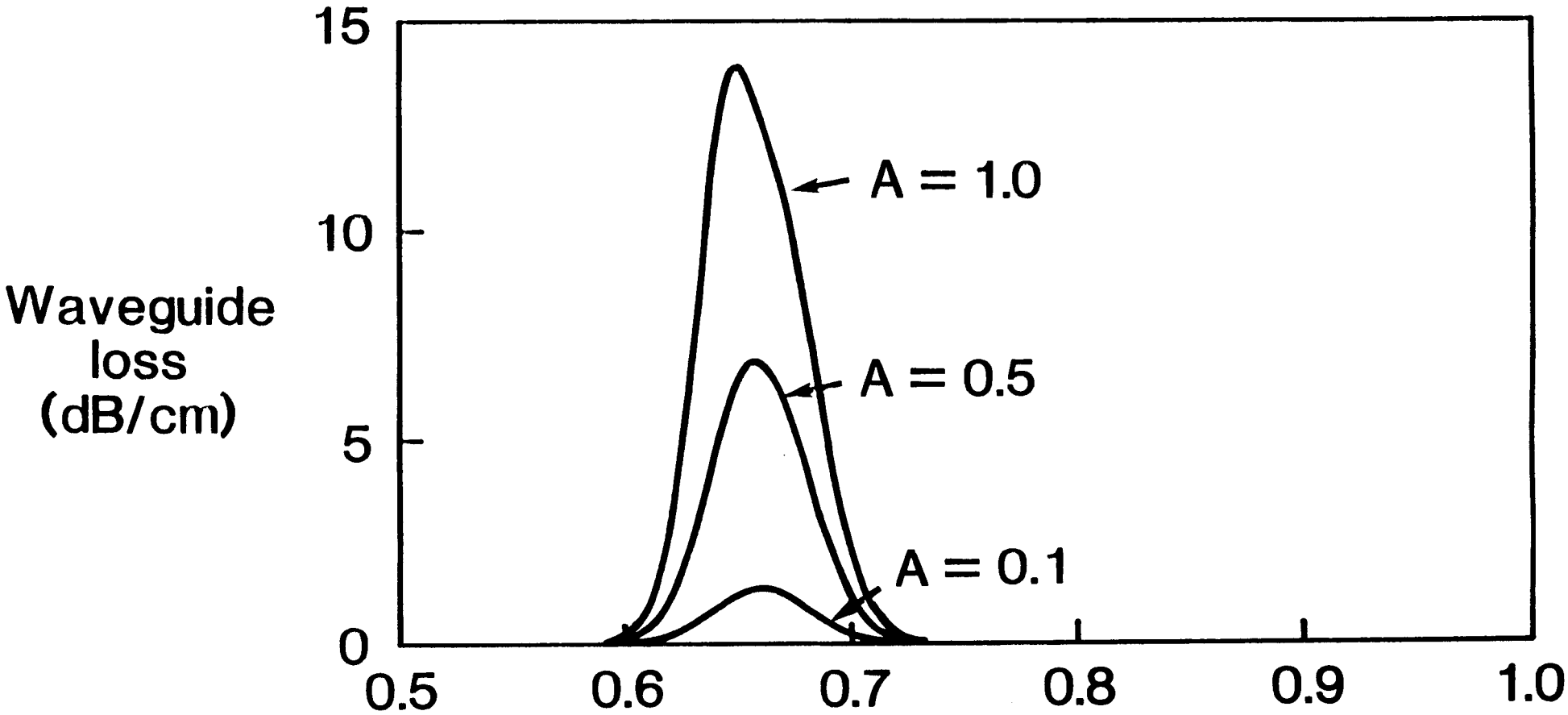
Waveguide loss (dB/cm)
15
10
5
0
0.5
0.6
0.7
0.8
0.9
1.0
A = 1.0
A = 0.5
A = 0.1

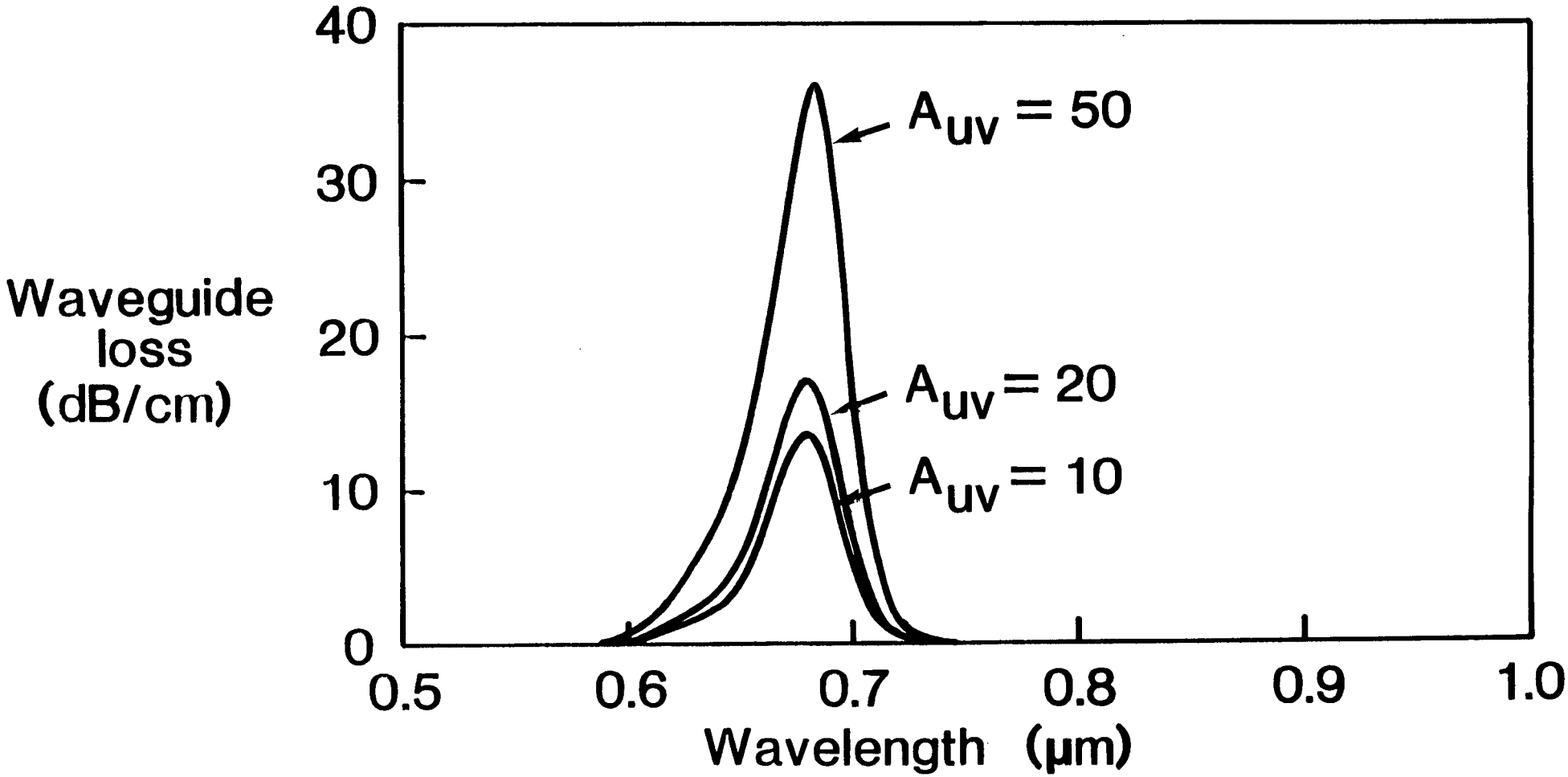
Waveguide loss (dB/cm)
40
30
20
10
0
A_{uv} = 50
A_{uv} = 20
A_{uv} = 10
0.5
0.6
0.7
0.8
0.9
1.0
Wavelength (μm)

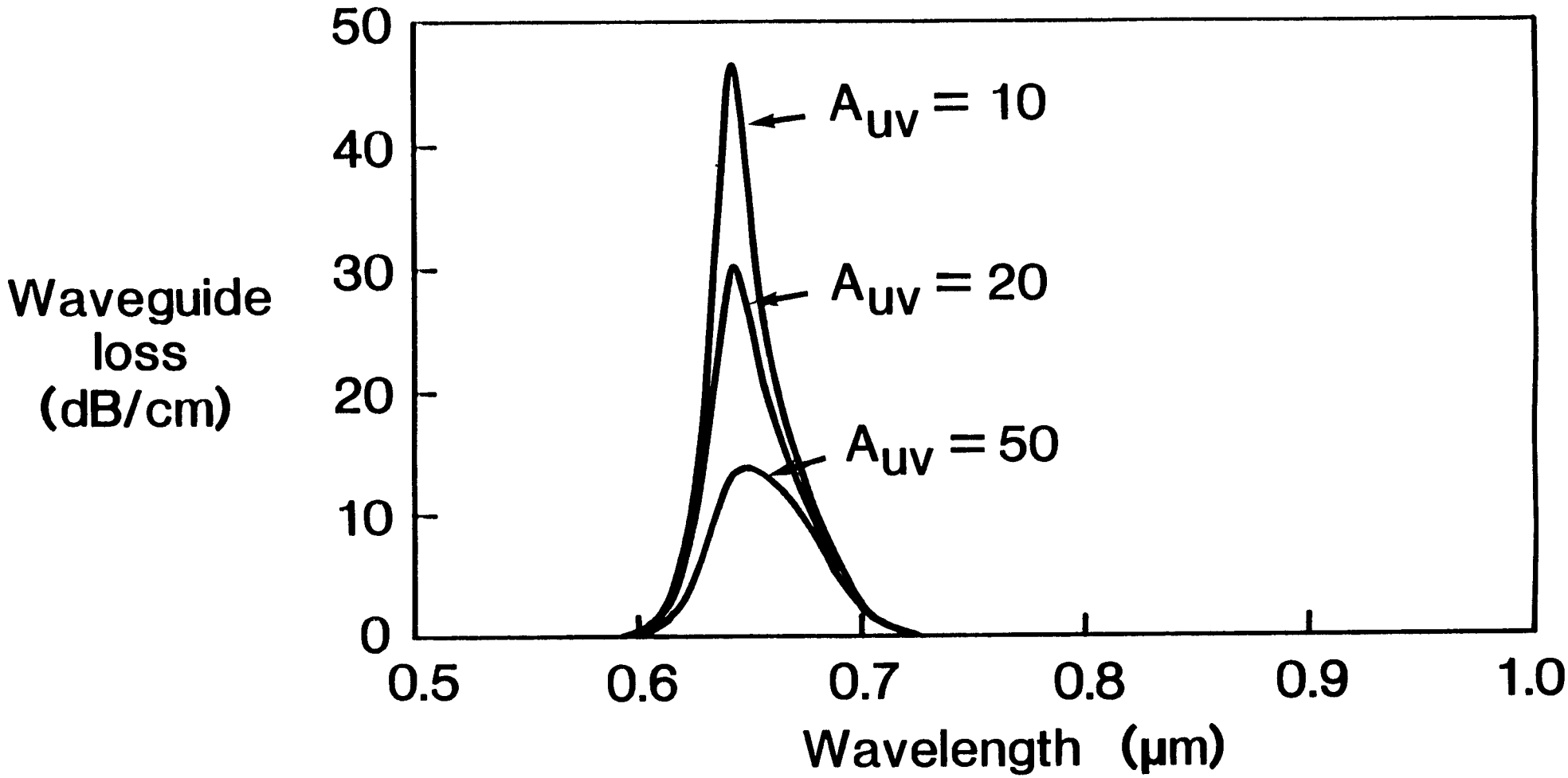
Waveguide loss (dB/cm)
50
40
30
20
10
0
$A_{uv} = 10$
$A_{uv} = 20$
$A_{uv} = 50$
0.5
0.6
0.7
0.8
0.9
1.0
Wavelength (μm)

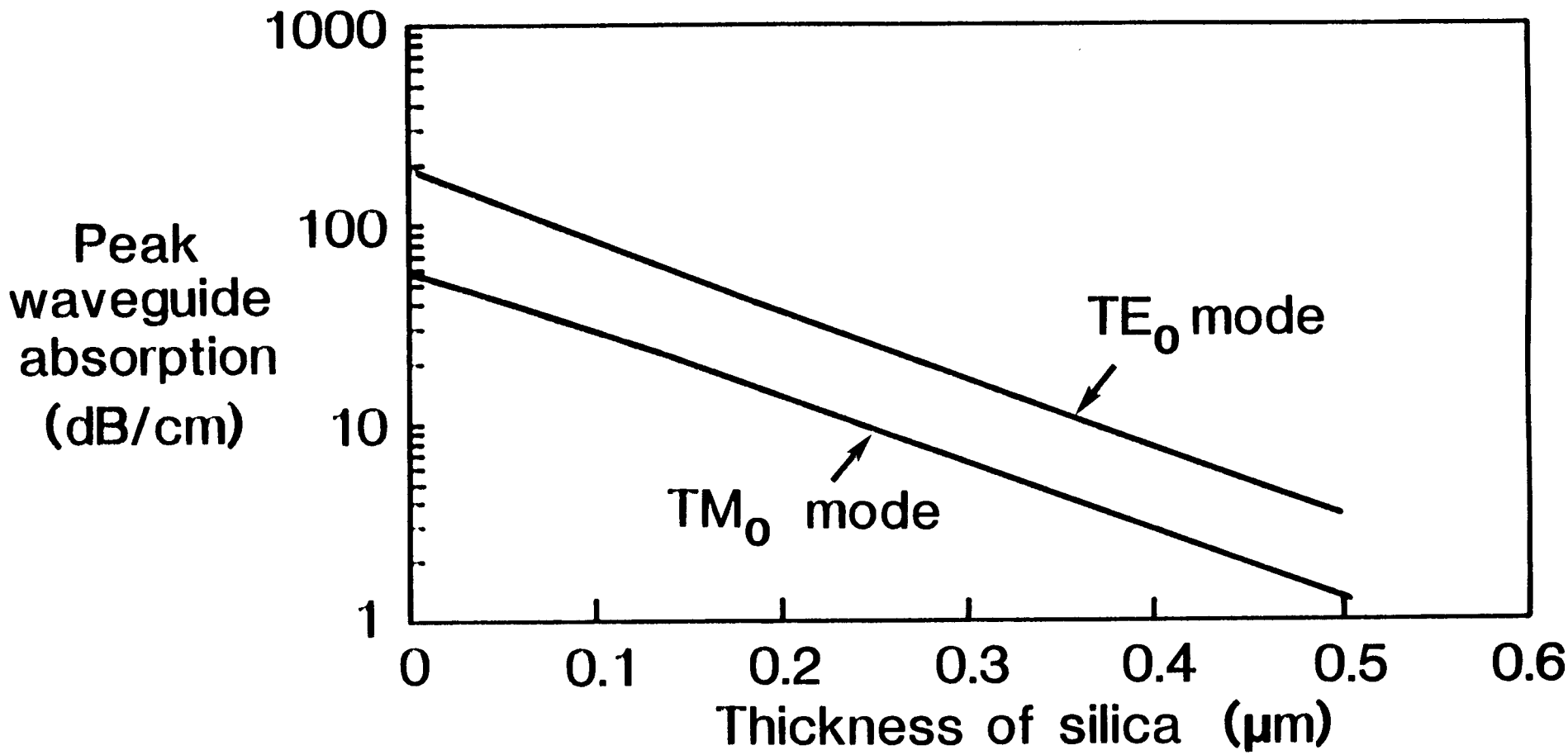
1000
100
10
1
Peak waveguide absorption (dB/cm)
TE0 mode
TM0 mode
0
0.1
0.2
0.3
0.4
0.5
0.6
Thickness of silica (μm)

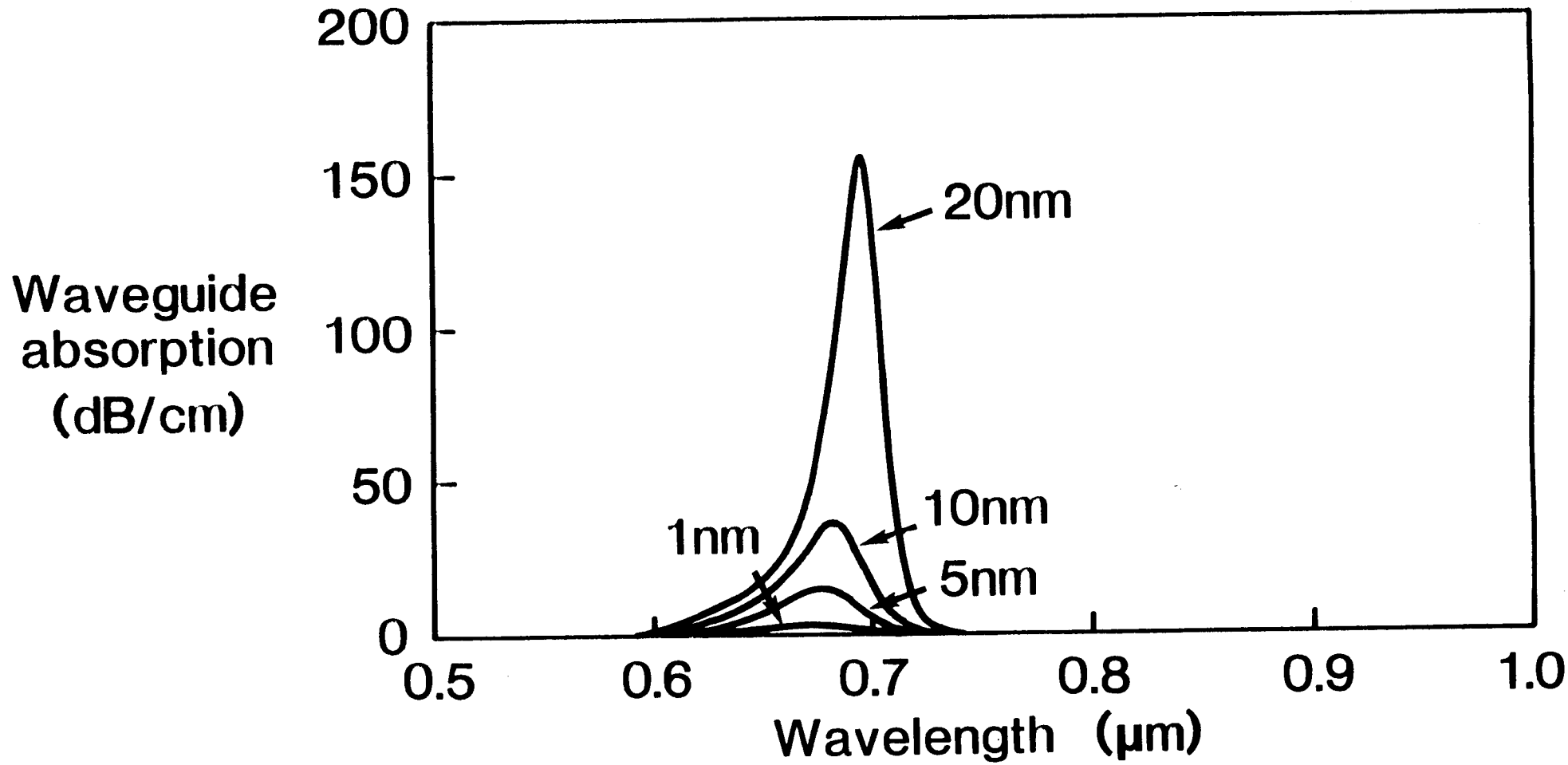
Waveguide absorption (dB/cm)
200
150
100
50
0
20nm
10nm
5nm
1nm
0.5
0.6
0.7
0.8
0.9
1.0
Wavelength (μm)

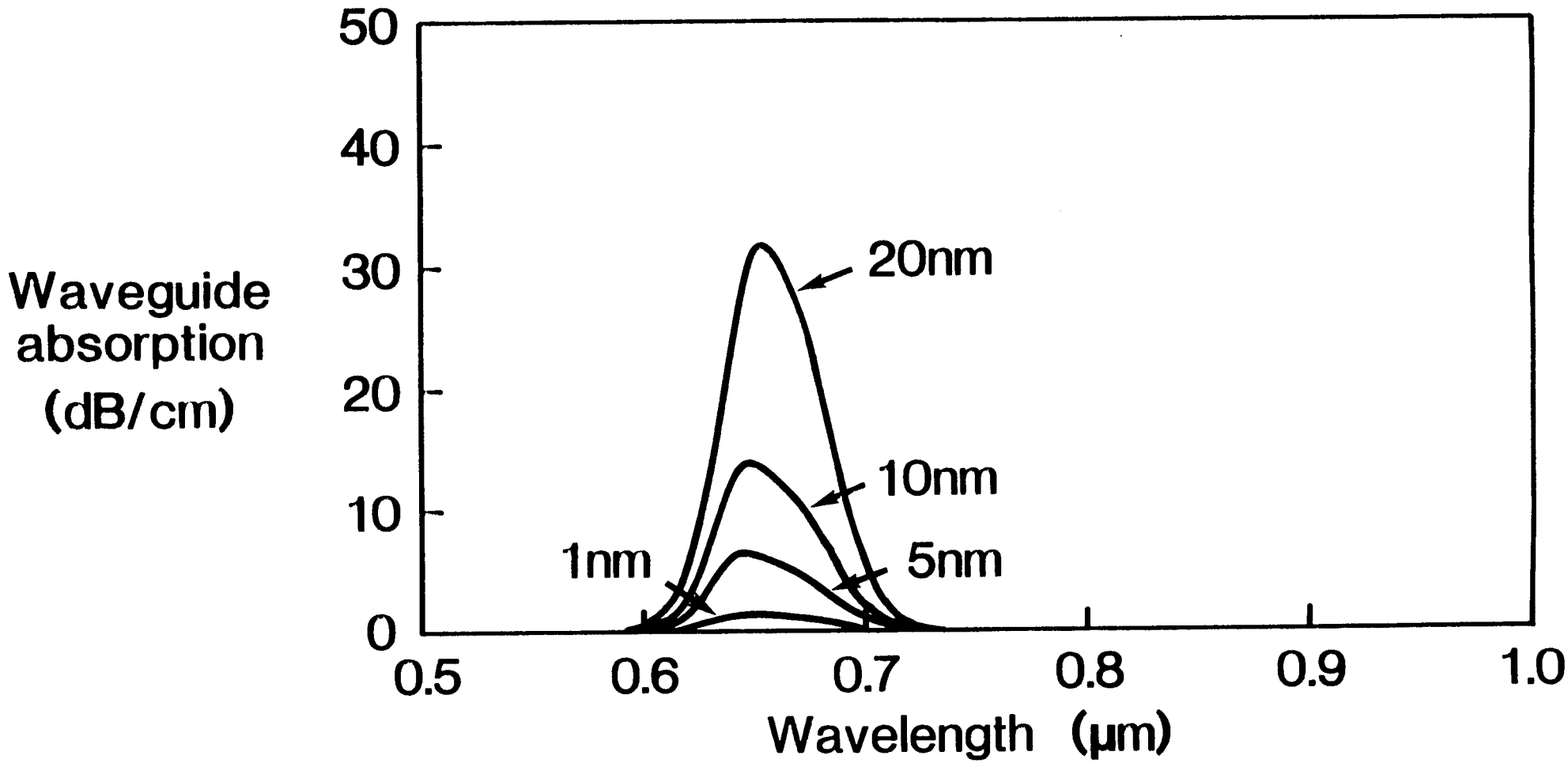
Waveguide absorption (dB/cm)
50
40
30
20
10
0
20nm
10nm
5nm
1nm
0.5
0.6
0.7
0.8
0.9
1.0
Wavelength (μm)

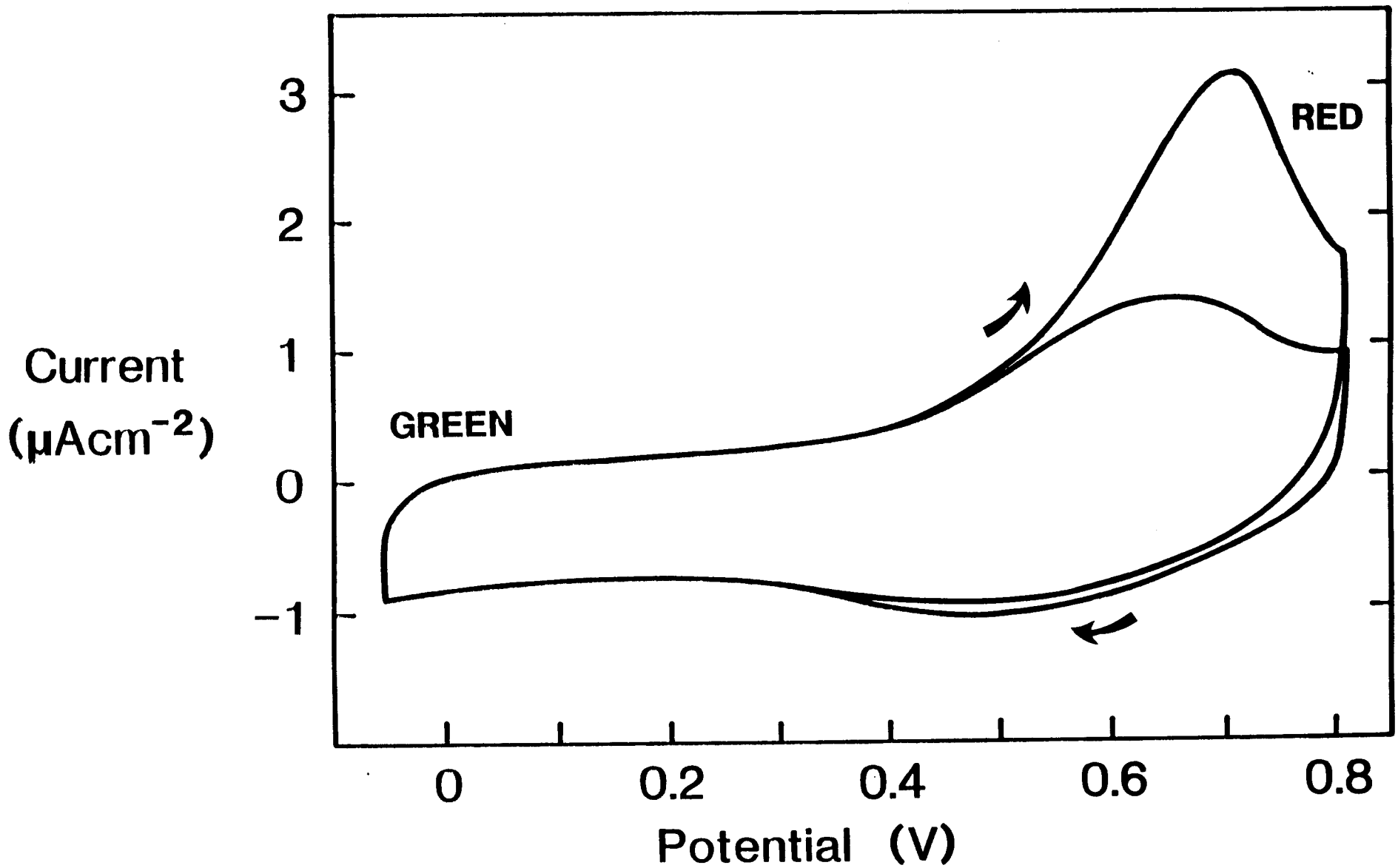
Current
(μAcm⁻²)
3
2
1
0
−1
GREEN
RED
0
0.2
0.4
0.6
0.8
Potential (V)

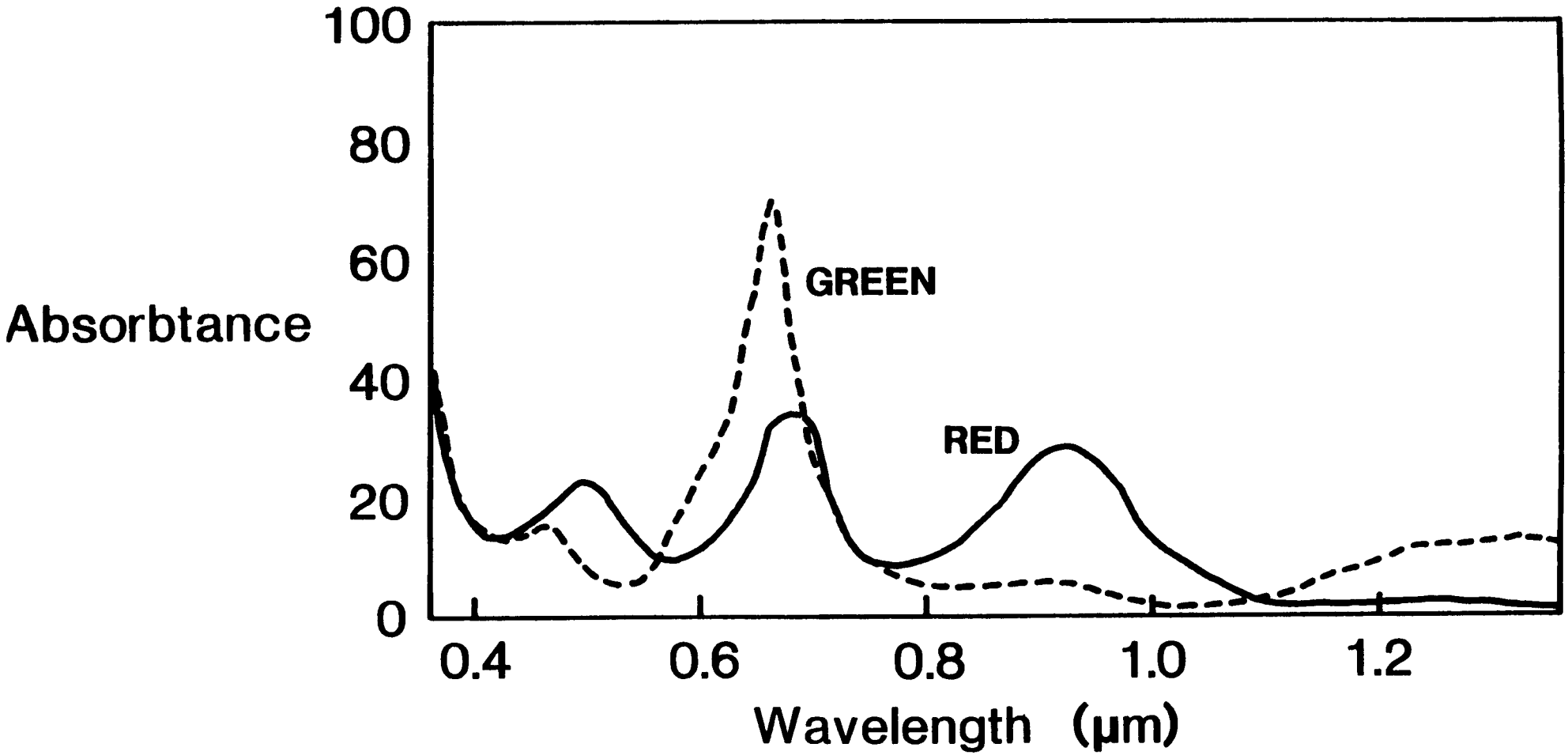
100
80
60
40
20
0
Absorbtance
GREEN
RED
0.4
0.6
0.8
1.0
1.2
Wavelength (μm)

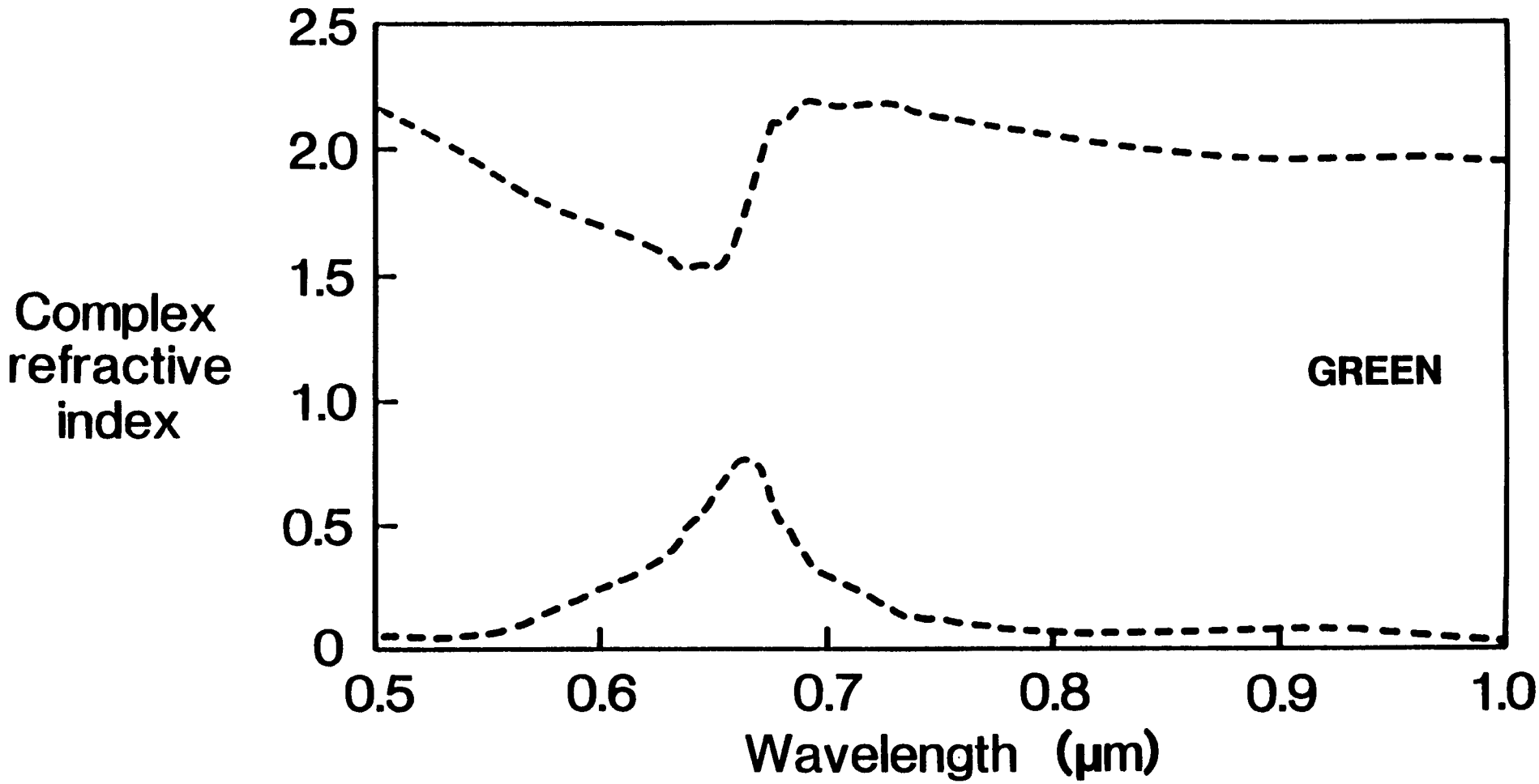
Complex refractive index
2.5
2.0
1.5
1.0
0.5
0
GREEN
0.5
0.6
0.7
0.8
0.9
1.0
Wavelength (μm)

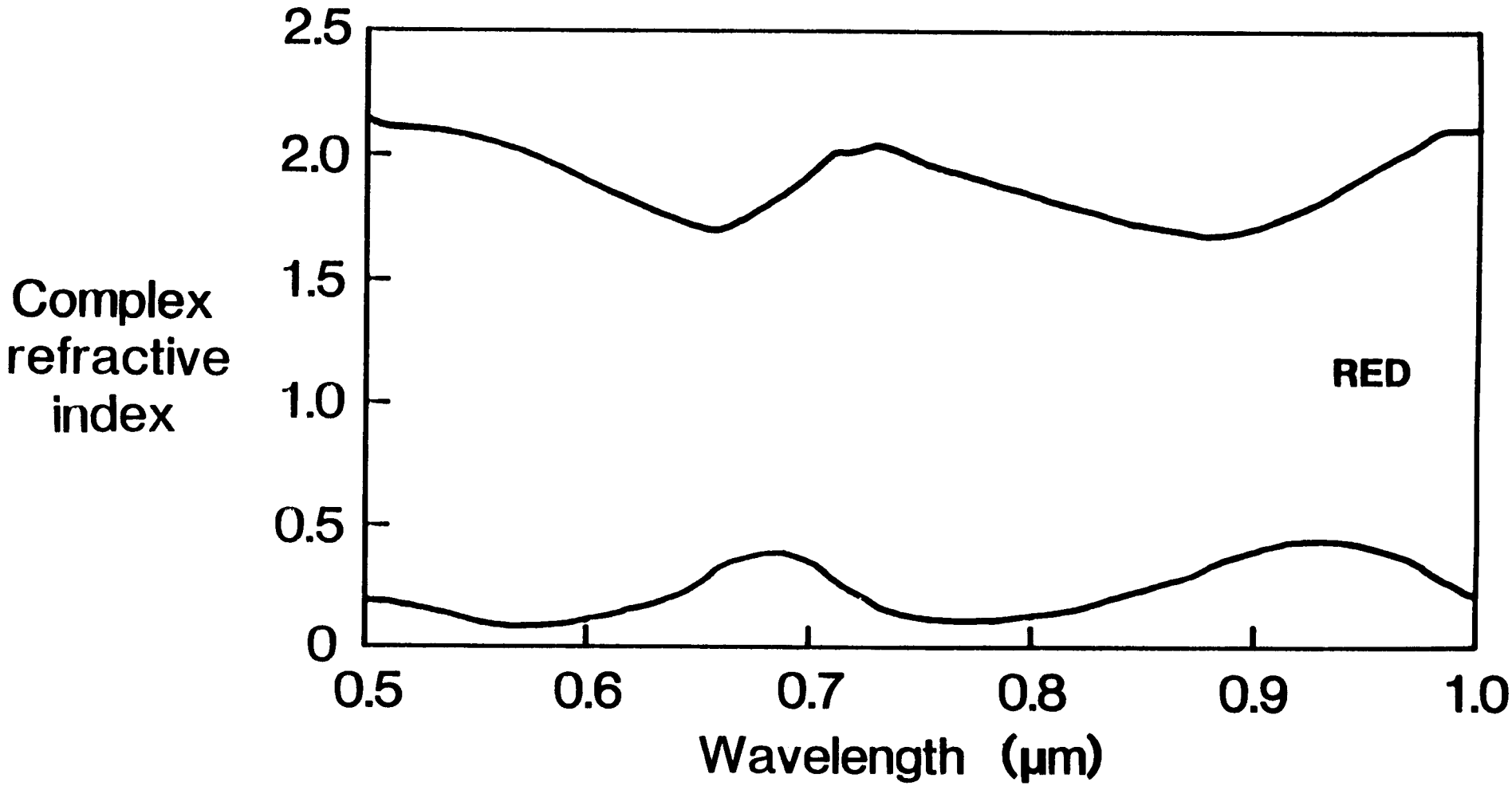
Complex refractive index
2.5
2.0
1.5
1.0
0.5
0
RED
0.5
0.6
0.7
0.8
0.9
1.0
Wavelength (μm)

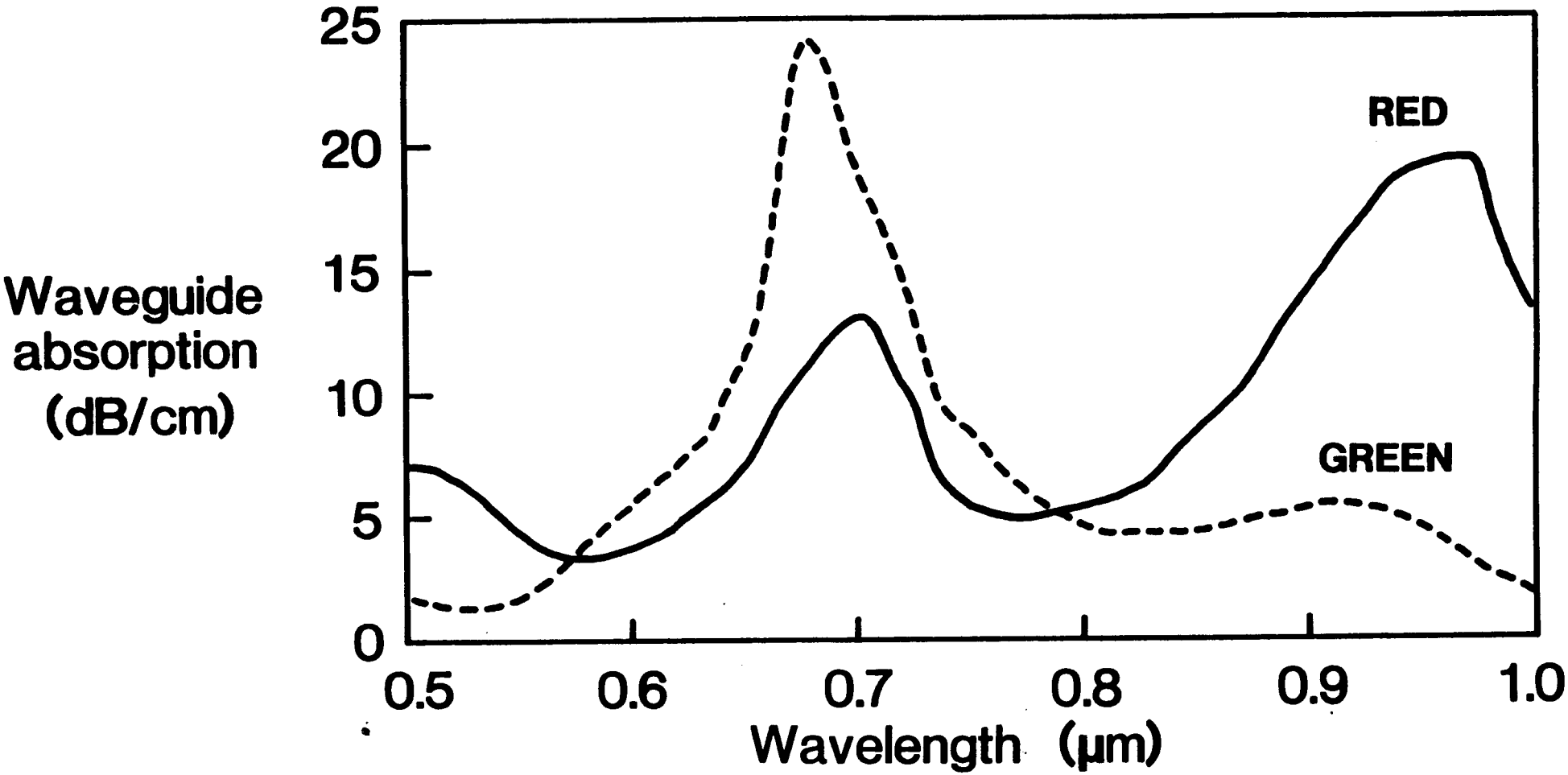
Waveguide absorption (dB/cm)
25
20
15
10
5
0
RED
GREEN
0.5
0.6
0.7
0.8
0.9
1.0
Wavelength (μm)

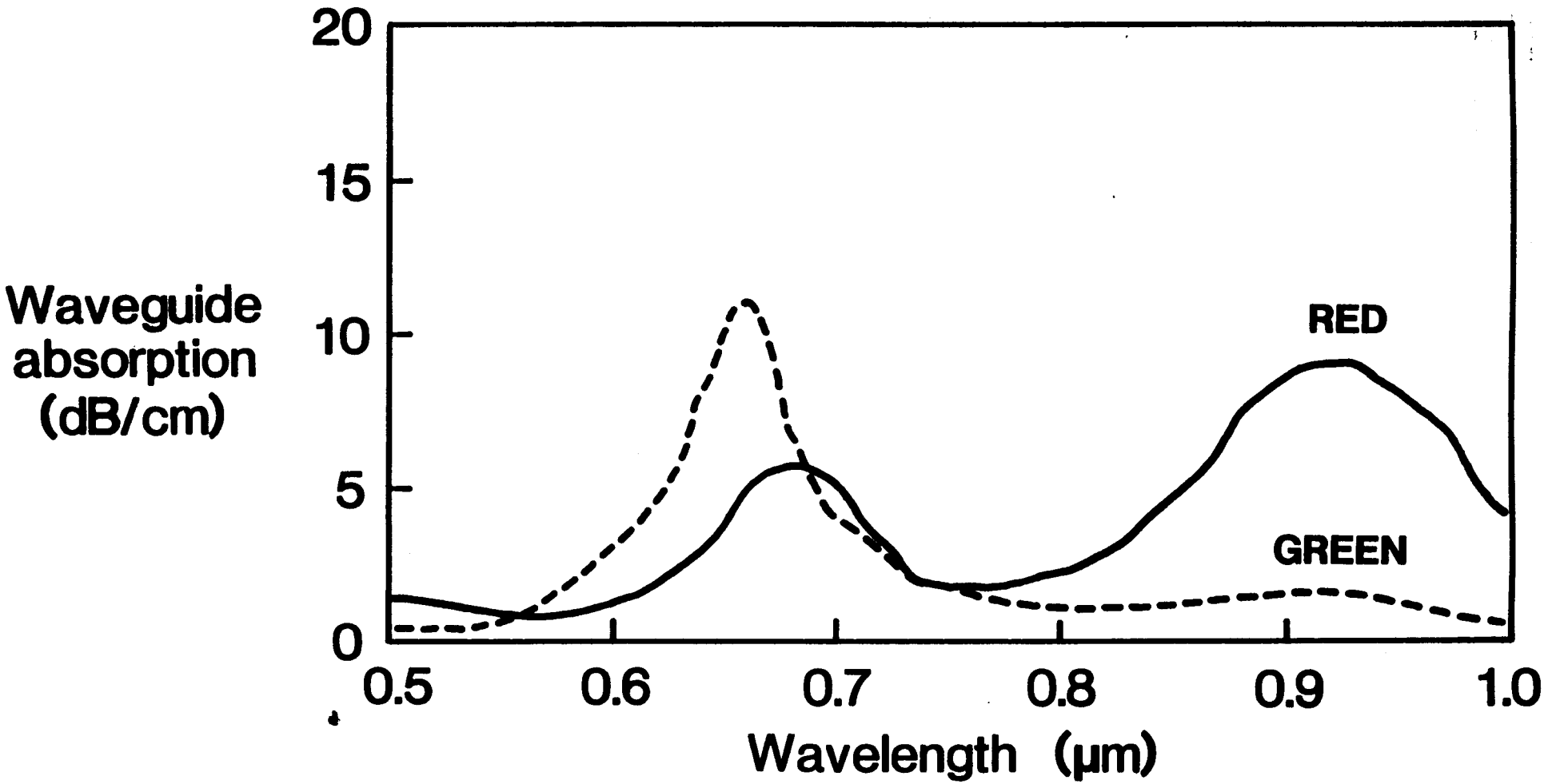
Waveguide absorption (dB/cm)
20
15
10
5
0
RED
GREEN
0.5
0.6
0.7
0.8
0.9
1.0
Wavelength (μm)

Fig 96

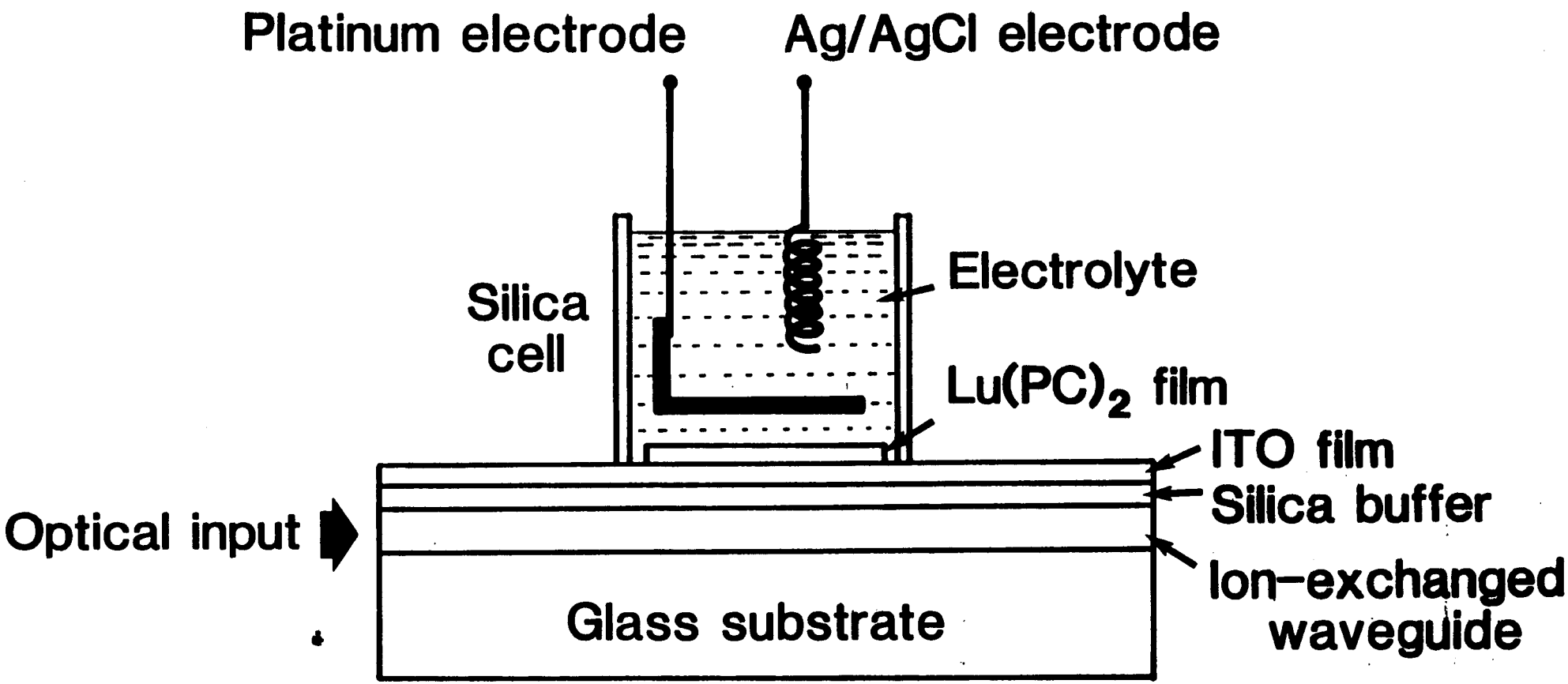
Platinum electrode
Ag/AgCl electrode
Silica cell
Electrolyte
Lu(PC)2 film
ITO film
Silica buffer
Optical input
Ion-exchanged waveguide
Glass substrate

Fig 10

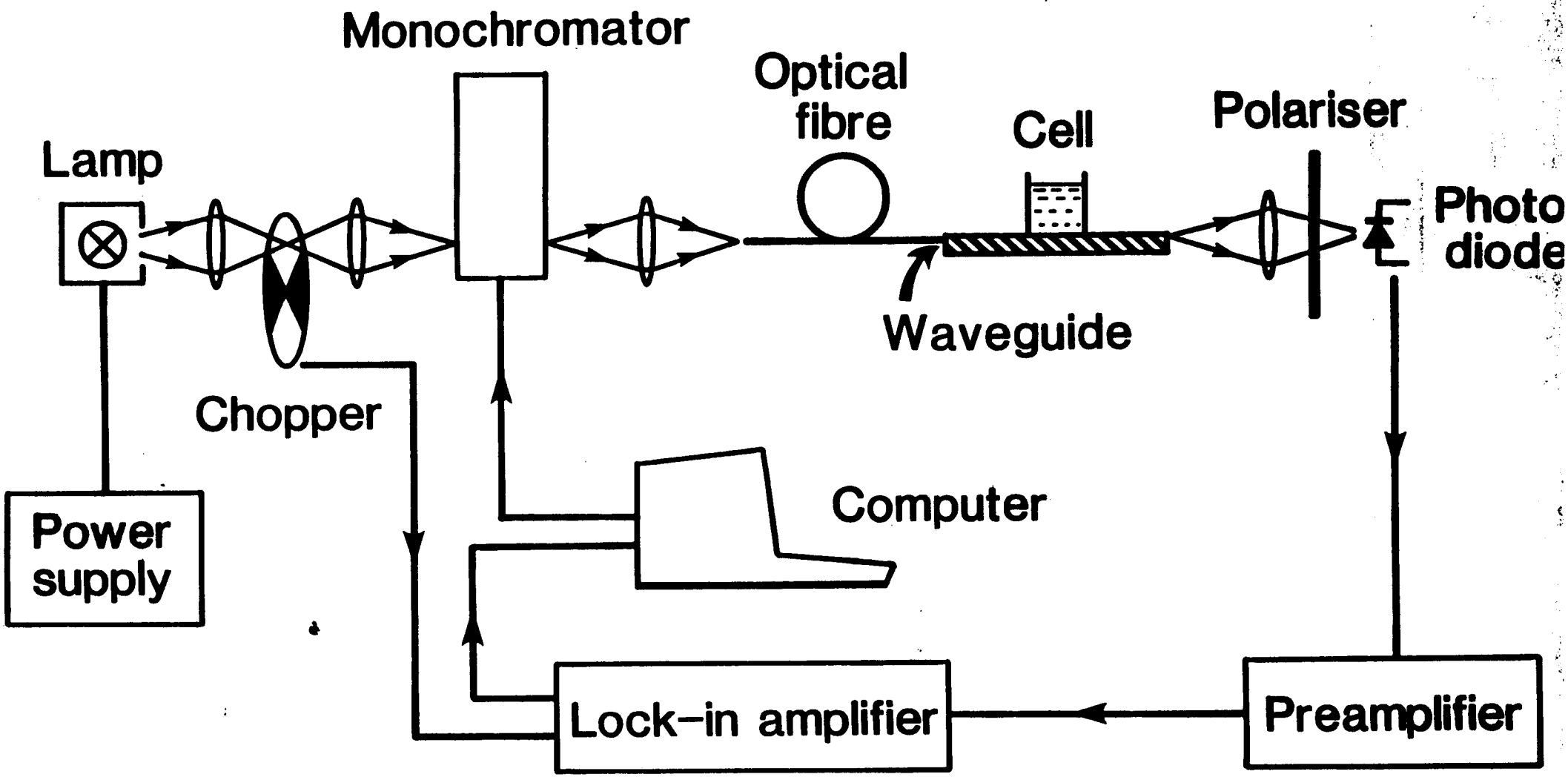
Monochromator
Optical fibre
Cell
Polariser
Lamp
Photo diode
Waveguide
Chopper
Computer
Power supply
Lock-in amplifier
Preamplifier

Fig 11

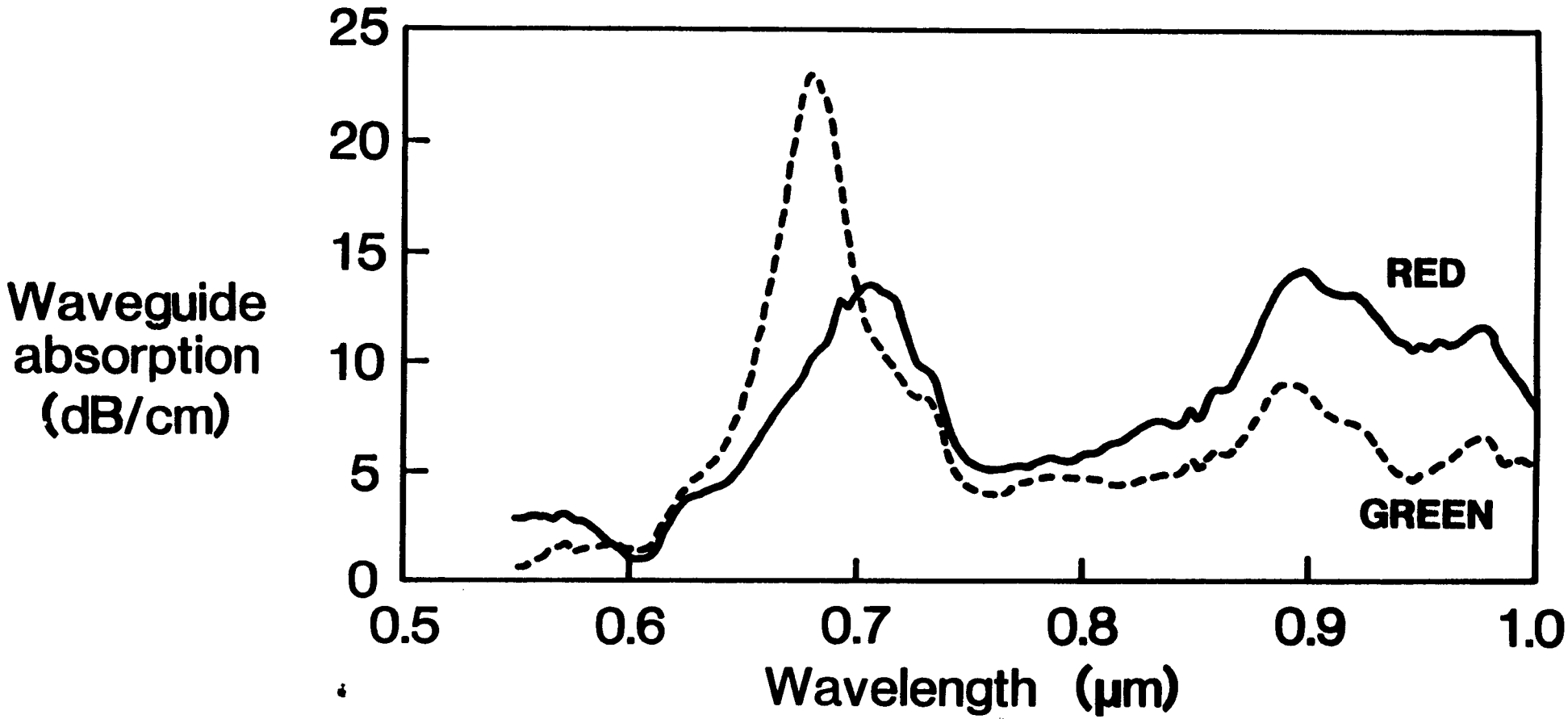
Waveguide absorption (dB/cm)
25
20
15
10
5
0
0.5
0.6
0.7
0.8
0.9
1.0
Wavelength (μm)
RED
GREEN

Fig 12a

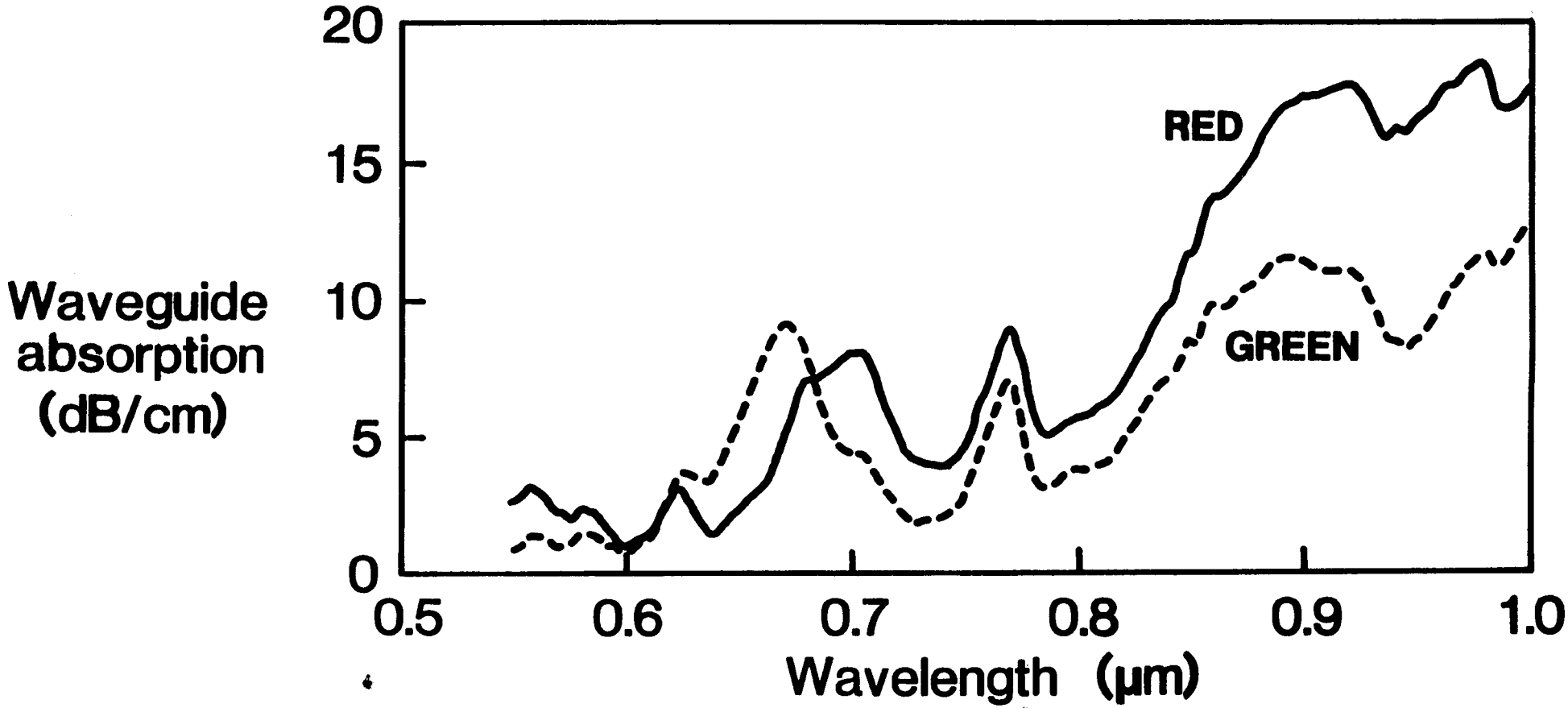
Waveguide absorption (dB/cm)
20
15
10
5
0
RED
GREEN
0.5
0.6
0.7
0.8
0.9
1.0
Wavelength (μm)

fig 12 b